This paper describes objective technical results and analysis. Any subjective views or opinions that might be expressed in the paper do not necessarily represent the views of the U.S. Department of Energy or the United States Government.

SAND2018-9065J

Total-internal-reflection elastic metasurfaces: design and application to structural vibration isolation

Hongfei Zhu,[1,*] Timothy F. Walsh,[2,†] and Fabio Semperlotti[1,‡]

[1] *Ray W. Herrick Laboratories, School of Mechanical Engineering, Purdue University, West Lafayette, Indiana 47907, USA*

[2] *Sandia National Laboratory, Albuquerque, New Mexico 87185, USA*

This letter presents the concept of Total Internal Reflection metasurface (TIR-MS) which supports the realization of structure-embedded subwavelength acoustic shields for elastic waves propagating in thin waveguides. The proposed metasurface design exploits extreme phase gradients, implemented via locally resonant elements, in order to achieve operating conditions that are largely beyond the critical angle. Such artificial discontinuity is capable of producing complete reflection of the incoming waves regardless of the specific angle of incidence. From a practical perspective, the TIR-MS behaves as a sound hard barrier that is impenetrable to long-wavelength modes at a selected frequency. The TIR metasurface concept is first conceived for a flat interface embedded in a rectangular waveguide and designed to block flexural A_0-type guided modes. Then, it is extended to circular plates in order to show how enclosed areas can be effectively shielded by incoming waves. This study shows numerical and experimental evidence that significant vibration isolation can be achieved under any arbitrary incidence angle when the metasurface is excited at the target frequency. Such results open new interesting paths to achieve vibration isolation and energy filtering in certain prototypical structures of interest for practical engineering applications.

I. INTRODUCTION

The concept of metasurface has recently emerged as a powerful approach to achieve compact and subwavelength devices for wave manipulation. The fundamental idea was first pioneered in optics [1–8] and later extended to acoustics [9–18]. At the basis of the metasurface design lies the concept of Generalized Snell's Law (GSL) [1, 19] that allows predicting the anomalous refraction across interfaces characterized by a phase gradient. Metasurfaces are rather versatile objects given the variety of phase shift profiles that can be encoded and that lead to remarkable and unconventional wave manipulation effects. A few examples include bending wave fields (either light or sound) in arbitrary shapes [2, 8], converting propagating into surface modes [7], and designing ultra-thin lenses [5, 6].

Only very recently, this concept was extended for application to elastodynamics [20–27] in order to control the refraction of elastic waves in solid waveguides. In their initial study, Zhu *et al.* [20] explored the behavior of an elastic metasurface in transmission mode and investigated the possibility of controlling the angle of refraction and the shape of an incoming planar wave front.

In traditional problems of wave transmission across an interface between dissimilar materials, both the angles of reflection and refraction are controlled by either the angle of incidence of the incoming wave or by the impedance mismatch between the two materials. For a given material selection, it is well-known that upon increasing the angle of incidence of the incoming wave a condition will be reached in which the wave cannot propagate into the second material (i.e. no refracted wave solution can exist). This threshold value of the incident angle is referred to as *critical angle*. Typically, at the first critical angle the angle of refraction is 90°, therefore the wave travels along the interface with no transmission into the second material. If the angle of incidence is further increased beyond the critical value, the wave is entirely reflected into the same half space giving rise to a phenomenon known as *total internal reflection* (TIR). In analogy with this classical behavior of wave propagation through an interface, we highlight that also a metasurface can achieve critical angle conditions.

In this letter, we explore both theoretically and experimentally the design and performance of an elastic metasurface that is explicitly designed to operate in the TIR regime. Such design is particularly interesting because it provides a fully passive approach to embedded subwavelength sound-hard barriers capable of blocking the propagation of elastic waves in the host waveguide. It is anticipated that this effect could be exploited in a variety of devices such as, for example, structural notch filters or, more in general, to achieve vibration isolation and control.

In the following, we present the general conditions and a possible design necessary to achieve a TIR metasurface. We first validate numerically the design (on either a rectangular or a circular plate), then we present an experimental validation for the case of a circular plate assembled in a prototypical structure and illustrate how vibration isolation can be effectively achieved under highly

* zhu307@purdue.edu

† tfwalsh@sandia.gov; Sandia National Laboratories is a multimission laboratory managed and operated by National Technology and Engineering Solutions of Sandia, LLC., a wholly owned subsidiary of Honeywell International, Inc., for the U.S. Department of Energys National Nuclear Security Administration. With main facilities in Albuquerque, N.M., and Livermore, C.A., Sandia has major R&D responsibilities in national security, energy and environmental technologies, and economic competitiveness.

‡ To whom correspondence should be addressed: fsemperl@purdue.edu

Sandia National Laboratories is a multimission laboratory managed and operated by National Technology & Engineering Solutions of Sandia, LLC, a wholly owned subsidiary of Honeywell International Inc., for the U.S. Department of Energy's National Nuclear Security Administration under contract DE-NA0003525.

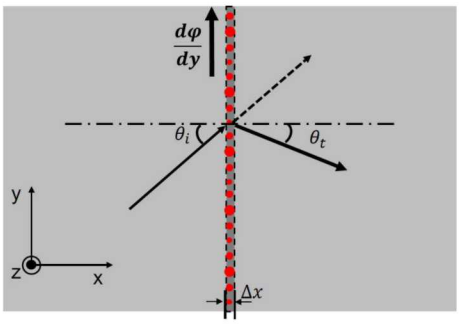

FIG. 1. Schematic view of an elastic waveguide with an embedded metasurface. Fundamental quantities such as the angle of incidence θ_i, the angle of refraction θ_t, and the phase gradient $\frac{d\phi}{dy}$ are shown.

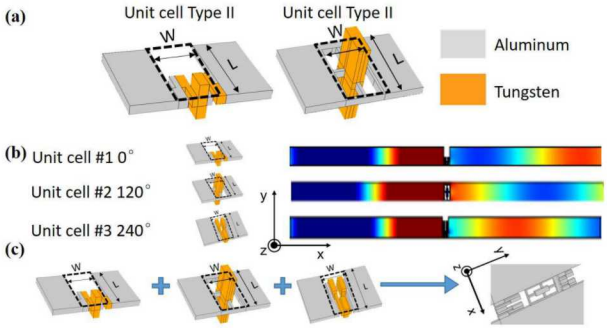

FIG. 2. Fundamental resonating unit cells of the TIR metasurface. (a) shows the schematics of the two unit cells used in our approach. The unit cells are designed based on either a space-coiling or a spring-mass approach and employ different materials (in the numerical example chosen to be aluminum and tungsten) in order to achieve the desired transfer function, while maintaining a compact design. (b) shows the in-plane displacement component of the S_0 wave traveling from left to right. The transmitted field has comparable amplitude and the required phase shift (in increments of 120°). (c) The three selected unit cells can be assembled in a supercell that covers a 2π phase shift. Then, the supercell is periodically repeated to assemble the complete metasurface.

subwavelength excitation conditions.

II. DESIGN OF THE METASURFACE FOR TOTAL INTERNAL REFLECTION

According to the Generalized Snell's Law (GSL) [1, 20], when an interface between two (either identical or different) media is encoded with a phase gradient $d\phi/dy$ (see Fig. 1), the direction of the refracted beam θ_t can be related to the incident angle θ_i as follows:

$$\frac{sin(\theta_t)}{\lambda_t} - \frac{sin(\theta_i)}{\lambda_i} = \frac{1}{2\pi}\frac{d\phi}{dy} \tag{1}$$

Equation (1) implies that, even when the two media are exactly identical ($\lambda_i = \lambda_t$), the direction of the refracted beam can be conveniently controlled by properly embedding a constant phase-gradient ($d\phi/dy$) along the direction of the interface. Given that in order to achieve propagating conditions across the interface (i.e. real-valued wave numbers $k_t = 2\pi/\lambda_t$)) it must be $-1 < sin(\theta_t) < 1$, any choice of the phase gradient that violates this condition will result in total internal reflection. Substituting this condition into Eq. (1), we obtain that in order to achieve TIR the phase gradient must satisfy the inequality $\frac{d\phi}{dy} \geq \frac{4\pi}{\lambda}$.

To achieve subwavelength control on the phase gradient, the metasurface employs locally resonant units [20] that are specifically tuned to provide a transfer function yielding the required phase shift along the interface direction. Note that each resonating unit provides a prescribed and constant change in phase, so the gradient $d\phi/dy$ is effectively discretized as a step-like function along the interface. Note that, not only the phase but also amplitude of the transfer function of the resonant unit plays an important role in determining the overall wave control because it determines the local magnitude of the reflected wave front and, hence, its homogeneity.

Previous studies on "transparent" metasurfaces (i.e. those interfaces designed to transmit waves at selected angles of refraction) showed that the amplitude of the transfer function of the different units forming the interface should be as large as possible and comparable with each other in order to preserve a constant wave amplitude along the wave front. Similarly, in TIR metasurfaces the amplitude of the transfer function should be uniform across different units and as low as possible in order to achieve an opaque or fully reflective interface.

In this study, the basic resonant unit (Fig.2a) is made by a rectangular block ($W = 40\ mm \times L = 80\ mm \times T = 8\ mm$) connected to a more elaborate internal structure. The latter is designed either according to the idea of space-coiling or of a simple spring-mass system (see details in Supplementary). It is worth noting that both add-on masses and dissimilar materials (in the numerical model chosen to be aluminum and tungsten) are employed in order to tune the resonance while maintaining a compact design.

Based on these two different designs, we assembled a metasurface capable of total internal reflection under a S_0 excitation at normal incidence and at a target frequency $f = 4.1$ kHz. The first step of the design requires assembling, from individual resonating units (Fig.2c), a supercell capable of providing the necessary phase gradient and amplitude profile. Three basic units having transmission coefficient ≈ 0.32 and phase shift difference of $2\pi/3$ between adjacent units were selected (see supporting material). The effect on the phase shift provided by each unit on the transmitted S_0 mode is shown in Fig.2b. The plots show the selected geometry for the resonant unit and the corresponding in-plane particle displacement pattern $U_x(x, y)$ at the neutral plane. Results clearly show a cumulative phase shift covering the whole 2π range. The latter is a required condition to guarantee

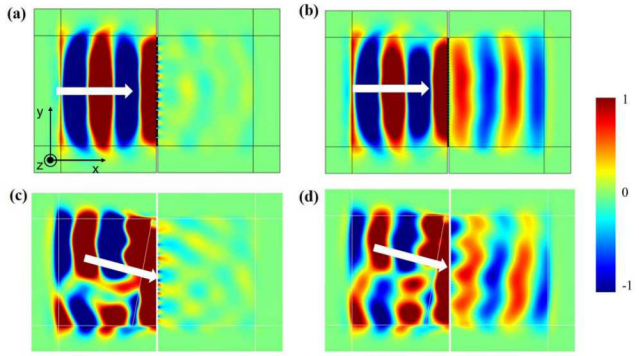

FIG. 3. Numerical simulations showing the response of the TIR metasurface embedded in a thin rectangular waveguide. (a) and (c) show the in-plane particle displacement component produced by the S_0 wave field under a S_0 input wave at normal and oblique incidence, respectively. (b) and (d) shows results analogous to (a) and (c) when the TIR-MS is replaced by a metasurface without phase gradient. The direct comparison of the results shows that the back scattering of the wave is not due to the impedance mismatch produced by the metasurface but it is instead due to the specific phase gradient profile.

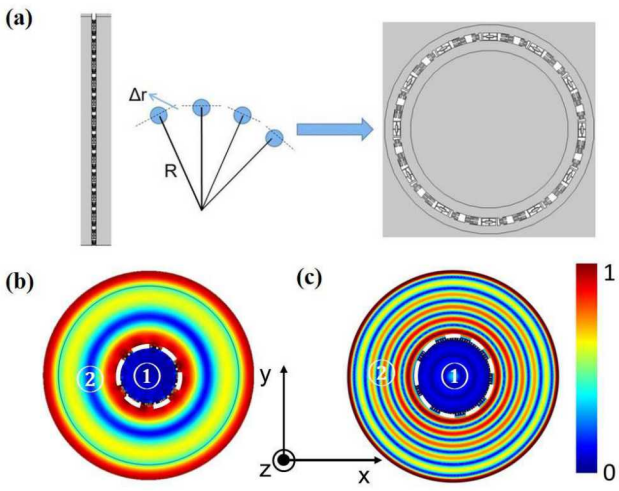

FIG. 4. (a) Conceptual schematic illustrating how the flat metasurface design could be adapted to create enclosed areas that are effectively shielded from unwanted mechanical energy. (b) Numerical simulation showing the normalized in-plane displacement component generated by a S_0 mode with circular wavefront generated at the outer boundary, traveling towards the center, and impinging on the TIR metasurface. The result show that most of the energy is blocked from transmitting through the metasurface at the target frequency of 4.1 kHz (i.e. energy propagating from zone ② does not reach zone ①). (c) Nnumerical simulation showing the out-of-plane displacement component generated by an A_0 mode with circular wavefront generated at the outer boundary, traveling towards the center, and impinging on the TIR metasurface. Most of the energy is blocked from transmitting through the metasurface (from zone ② to zone ①) at the target frequency of 0.5 kHz.

that, when multiple supercells are assembled in a periodic pattern to form the metasurface, the phase gradient evolves smoothly in increments that are integer multiple of 2π.

III. NUMERICAL SIMULATIONS

A. TIR metasurface for a rectangular waveguide

To illustrate the validity of the design and the performance of the metasurface in terms of total internal reflection, we embedded the TIR metasurface in a thin aluminum rectangular waveguide having thickness $T = 8\ mm$ (Fig.2c). The corresponding numerical model was assembled and solved in a commercial finite element software (COMSOL Multiphysics^{TM}). The target frequency was selected at $f = 4.1$ kHz and the phase increment between two adjacent units was $\det \phi = 2\pi/3$. This condition fulfills the requirement necessary to achieve TIR effects and provide a very subwavelength design as demonstrated by the ratio $\lambda/\Delta x \approx 12.5$, where Δx is the width of the metasurface as shown in Fig.1. The metasurface was excited by a S_0 planar wave traveling from left to right under two conditions: 1) normal incidence, and 2) oblique incidence ($\theta_i = 30°$).

Figure 3a and c show the in-plane displacement component produced by the S_0 guided mode after interaction with the TIR-MS at normal and oblique incidence (i.e. $\theta_i = 30°$), respectively. The superimposed white arrows indicates the incident wave direction. Results clearly show that most of the incident energy is back reflected while just a minor portion is refracted through the metasurface. This transmitted scattered field is due to the discretized nature of the interface (i.e. the openings between adjacent units) and resemble a typical slit diffraction effect.

To further illustrate the performance of the TIR metasurface, we simulated the propagation conditions in an equivalent waveguide (indicated below as reference configuration) where the TIR-MS was replaced by a geometrically equivalent metasurface. The latter interface has the same transmission amplitude than the TIR-MS but it does not implement the phase shift gradient. Such metasurface can be easily assembled by repeating only one of the basic unit cells along the $y-$direction. The intent of this comparison is to show that the back reflection of the incident wave is not due to a simple impedance mismatch but instead to the actual design of the TIR interface.

The numerical results of the reference configuration are shown in Fig.3b and d for the two incidence angles. The results are still presented in terms of in-plane particle displacement of the S_0 wave field. By direct comparison with Fig.3a and c, it is evident that although some back reflections due to the impedance mismatch certainly occurs, only the TIR design is capable of blocking the wave under this very challenging subwavelength conditions.

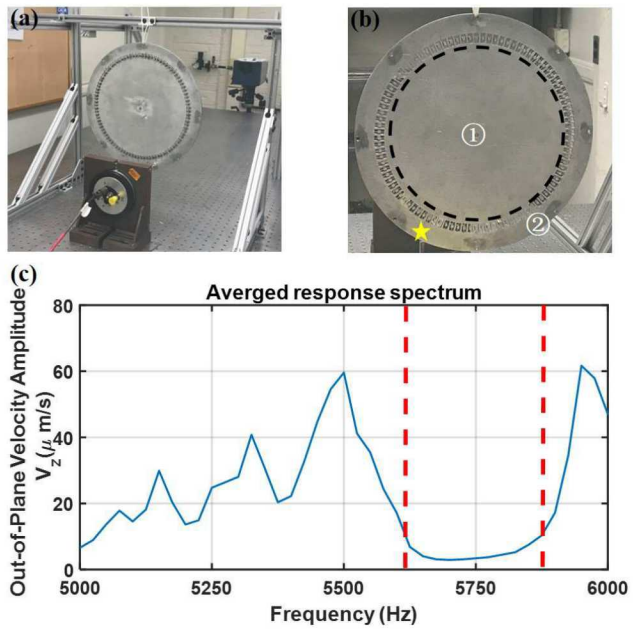

FIG. 5. Experimental setup. The plate was tested under free boundary conditions implemented by suspending the plate from an external aluminum frame. The excitation was provided by a piezoelectric shaker connected to the outer region, as indicated in (a). (a) and (b) show the rear and front view of the set-up. (c) shows the spatially-averaged (out-of-plane) velocity spectrum obtained from all the points internal to the metasurface (i.e. zone ①). The spectrum was measured under white noise excitation covering the bandwidth 5-6 kHz. The measurements show a strong reduction in the transmitted energy within zone ① around $f = 5.75$ kHz, which is the approximate operating frequency of the metasurface.

B. TIR metasurface for a circular waveguide: application to vibration isolation

From the results presented above, it appears that the TIR-MS is particularly well suited for blocking the propagation of wave fronts under highly subwavelength conditions and, eventually, to create analog notch filters that block a selected frequency. To illustrate this specific capability of the TIR-MS, we show the application of this concept to a thin circular waveguide. The underlying idea being that one wants to create fully enclosed areas shielded by incoming waves at a given frequency but with any angle of incidence. In order to directly extend the results from the previous section, we can envision bending the flat TIR-MS into a circular pattern closed on itself in such a way to divide the plate into two concentric regions. To achieve this result each unit was distributed over an arc of a circle. This approximation works well as far as $R \gg \delta r$, where R is the radius of the circular metasurface and δr is the distance between two adjacent units. Under such condition, the change in the direction of the local tangent at neighboring sites can be neglected and the phase gradient can be approximated as $d\phi/\Delta r$.

In order to illustrate this concept, we designed a circular TIR metasurface based on the unit cells designed above. The circular TIR-MS consisted of twelve complete supercells (having three unit cells each) having a radius $R = 18 * L/\pi$. The metasurface was fully embedded in a circular plate dividing it in an inner circular area (the region to be isolated from incoming waves, labeled zone ① in Fig.4b and c) and an outer annular ring (the region where the incoming wave is generated, labeled zone ② in Fig.4b and c). The plate was excited on its most outer boundary using a S_0 wave at the target frequency $f = 4.1$ kHz. The dynamic response of the system is presented in Figure 4b in terms of the in-plane displacement at the mid-plane. As expected, the incident energy is almost entirely back reflected and the inner circular plate is efficiently isolated from the incoming wave.

It is worth mentioning that, although the operating mechanism of the TIR-MS was exemplified using a S_0 wave type, the design approach remains identical should the metasurface be designed to isolate A_0 wave type. This statement is supported by a numerical example that shows how the same circular plate could be redesigned to isolate the center region (zone ①) from incoming A_0 waves. Naturally, the basic unit cells were re-designed to operate at a new target frequency $f = 0.5$ kHz which was selected to target a subwavelength regime for the A_0 mode. Figure 4c shows the out-of-plane displacement component of the A_0 wave field when the circular TIR metasurface is excited by an incoming A_0 wave generated at the outer plate boundary (zone ②). Also in this case, the results clearly show the TIR effect for the A_0 mode. The details of the geometric configuration are discussed in supplementary material.

IV. EXPERIMENTAL VALIDATION

In order to validate the TIR-MS concept and evaluate its performance, we built an experimental test bed and measured its response using laser vibrometry. In particular, we reproduced the specific case of a circular TIR-MS designed to isolate its most inner area. To facilitate the fabrication and testing, we re-designed the metasurface by rescaling the basic unit and using as materials aluminum and steel. The rescaling procedure resulted in a target frequency of 5.5 kHz for the A_0 mode (the details of the geometry are reported in supplementary material). The circular TIR-MS was fabricated by waterjet cutting the slots starting from a uniform flat plate and then gluing the add-on masses.

The test setup is shown in Fig.5. The rear and front views of the whole setup are provided in Fig.5a and b. The plate was suspended from an aluminum frame in order to provide free boundary conditions while a piezoelectric shaker was connected to the outer area (see $\star$ in Fig.5b) in order to provide the necessary dynamic excitation. The goal of the metasurface is to dynamically isolate the internal region (zone ①) from the incoming waves generated in zone ②. The response of the plate was measured under white noise excitation (bandwidth 5-6 kHz) by using a PSV-500 laser vibrometer. Figure 5c

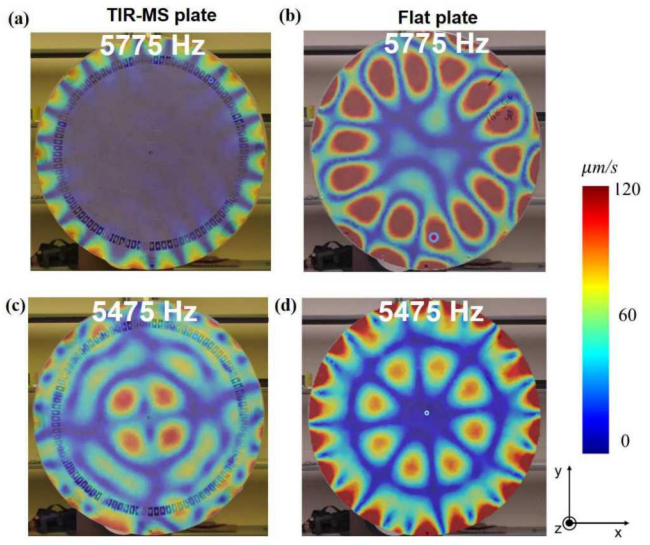

FIG. 6. Experimental results. (a) shows the response of the TIR-MS plate at the frequency $f = 5.775$ kHz inside the spectrum dip as shown in Fig.5c, where the vibration energies were well isolated by the metasurface while (b) shows the response of a flat plate under the same excitation condition as a comparison. (c) shows the response of the MS-plate at a detuned frequency $f = 5.475$ kHz outside the dip while (c) shows the response of a flat plate under the same excitation condition.

presents the amplitude of the spatially-averaged velocity spectrum of the internal region (zone ①). The large drop in the amplitude of the spectrum in the frequency band $5.65 - 5.85$ kHz identifies the region in which the metasurface is operating (around a center frequency of approximately 5.75 kHz). This frequency is only 250 Hz off the numerically predicted target frequency, that is a 4% error. This is considered a negligible discrepancy and it is associated with fabrication tolerances on both the individual unit cell slots and the add-on masses.

Figure 6 summarizes the results of the experimental measurements. In particular, Fig. 6a and b show the response of the TIR-MS and of the reference flat plates at the frequency $f = 5.775$ kHz within the operating range of the metasurface (see dashed lines in Fig.5c). The response is measure in terms of out-of-plane velocity V_z amplitude distribution. As expected, in the TIR-MS plate the vibrational energy is confined outside the metasurface, resulting in the formation of a lobbed pattern while leaving the internal region almost completely unaffected. On the contrary, in the case of the flat plate (Fig.6b) the excitation produces a pattern resembling a global vibration mode for the most part localized in the equivalent internal area of the metasurface. In order to provide a quantitative comparison of the effect of the metasurface in terms of energy isolation, we calculated the amplitude of the spatially-average velocity spectrum in zone ① and ②, labeled as V_{z1} and V_{z2}. For the TIR-MS plate $V_{z1}^{MS} = 5.29\ \mu m/s$ and $V_{z2}^{MS} = 52.84\ \mu m/s$, while for the flat plate plate $V_{z1}^{flat} = 182.11\ \mu m/s$ and $V_{z2}^{flat} = 192.14\ \mu m/s$. The direct comparison of this quantity shows that most of the energy is confined in zone ② in the case of the TIR-MS while it reaches zone ① for the flat plate.

For completeness, we also report the response of the two plates for a slightly detuned frequency $f = 5.475$ kHz, that is outside the operating range of the TIR-MS (i.e. outside the dashed lines in Fig.5c). A direct comparison of the velocity spectra (Fig.6c and d) shows that the vibrational energy can reach zone ① in both cases given that the excitation frequency cannot trigger the local resonator and hence activate the metasurface. The resulting vibration pattern is different in the two plates because the MS still behaves as an artificial boundary condition for the plate.

V. CONCLUSIONS

We have presented and experimentally validated the concept of total internal reflection elastic metasurface (TIR-MS) which is capable of highly subwavelength dynamic isolation. The TIR-MS relies on the existence of critical phase shift gradients which guarantee that incident wave fronts at any arbitrary angle cannot be transmitted in the region downstream of the engineered interface. The specific metasurface design employs locally resonant units capable of achieving large phase shifts covering the whole 2π range under highly subwavelength conditions. Effective wave control was shown first numerically and then experimentally on different thin elastic waveguides. While traditional metasurfaces are typically designed to be transparent and refract waves in a controlled manner, the TIR-MS is designed to be opaque or, ideally, fully reflective. Results show that TIR-MS is particularly well suited for blocking the propagation of wave fronts with an arbitrary angle of incidence and at a selected frequency. This aspect of the TIR-MS is considered particularly convenient to create highly subwavelength vibration isolation while preserving the structural role of the host system. Given the narrow band characteristic of the resonant metasurface design, it is expected that the TIR-MS could also be employed as an analog notch filter to block a selected frequency.

VI. ACKNOWLEDGMENTS

The authors gratefully acknowledge the financial support of the Sandia National Laboratory under the Academic Alliance program, grant #1847039.

[1] N. Yu, P. Genevet, M. A. Kats, F. Aieta, J.-P. Tetienne, F. Capasso, and Z. Gaburro, Science **334**, 333 (2011).

[2] X. Ni, N. K. Emani, A. V. Kildishev, A. Boltasseva, and V. M. Shalaev, Science **335**, 427 (2012).

[3] N. K. Grady, J. E. Heyes, D. R. Chowdhury, Y. Zeng, M. T. Reiten, A. K. Azad, A. J. Taylor, D. A. R. Dalvit, and H.-T. Chen, Science **340**, 1304 (2013).

[4] C. Pfeiffer and A. Grbic, Phys. Rev. Lett. **110**, 197401 (2013).

[5] F. Aieta, P. Genevet, M. A. Kats, N. Yu, R. Blanchard, Z. Gaburro, and F. Capasso, Nano. Lett. **12**, 4932 (2012).

[6] M. Kang, T. Feng, H.-T. Wang, and J. Li, Opt. Express **20**, 15882 (2012).

[7] S. Sun, Q. He, S. Xiao, Q. Xu, X. Li, and L. Zhou, Nat. Mater. **11**, 426 (2012).

[8] L. Huang, X. Chen, H. Muhlenbernd, G. Li, B. Bai, Q. Tan, G. Jin, T. Zentgraf, and S. Zhang, Nano. Lett. **12**, 5750 (2012).

[9] Y. Li, B. Liang, Z. Gu, X. Zou, and J. Cheng, Sci. Rep. **3** (2013).

[10] Y. Li, X. Jiang, R.-q. Li, B. Liang, X.-y. Zou, L.-l. Yin, and J.-c. Cheng, Phys. Rev. Applied **2**, 064002 (2014).

[11] J. Mei and Y. Wu, New. J. Phys. **16**, 123007 (2014).

[12] K. Tang, C. Qiu, M. Ke, J. Lu, Y. Ye, and Z. Liu, Sci. Rep. **4** (2014).

[13] B. Yuan, Y. Cheng, and X. Liu, Appl. Phys. Express. **8** (2015).

[14] J. Zhao, B. Li, Z. Chen, and C. W. Qiu, Sci. Rep. **3** (2013).

[15] J. Zhao, B. Li, Z. N. Chen, and C.-W. Qiu, Appl. Phys. Lett. **103** (2013).

[16] Y. Zhu, X. Zou, R. Li, X. Jiang, J. Tu, B. Liang, and J.-C. Cheng, Sci. Rep. **5** (2015).

[17] K. Tang, C. Qiu, J. Lu, M. Ke, and Z. Liu, J. Appl. Phys. **117** (2015).

[18] Y. Li, X. Jiang, B. Liang, J.-c. Cheng, and L. Zhang, Phys. Rev. Applied **4**, 024003 (2015).

[19] N. Yu and F. Capasso, Nat. Mater. **13**, 139 (2014).

[20] H. Zhu and F. Semperlotti, Phys. Rev. Lett. **117**, 034302 (2016).

[21] Y. Liu, Z. Liang, F. Liu, O. Diba, A. Lamb, and J. Li, Phys. Rev. Lett. **119**, 034301 (2017).

[22] S. Li, J. Xu, and J. Tang, Applied Physics Letters **112**, 021903 (2018).

[23] X. Su, Z. Lu, and A. N. Norris, Journal of Applied Physics **123**, 091701 (2018).

[24] Journal of the Mechanics and Physics of Solids **112**, 577 (2018).

[25] Y. Xu, Z. Yang, and L. Cao, Journal of Physics D: Applied Physics **51**, 175106 (2018).

[26] X. Shen, C.-T. Sun, M. V. Barnhart, and G. Huang, Journal of Applied Physics **123**, 091708 (2018).

[27] S. Tol, Y. Xia, M. Ruzzene, and A. Erturk, Applied Physics Letters **110**, 163505 (2017).